International Journal of Pressure Vessels and Piping 111-112 (2013) 106–119

Contents lists available at SciVerse ScienceDirect

International Journal of Pressure Vessels and Piping

journal homepage: www.elsevier.com/locate/ijpvp

Effects of specimen geometry and loading mode on crack growth resistance curves of a high-strength pipeline girth weld

Leonardo L.S. Mathias, Diego F.B. Sarzosa, Claudio Ruggieri*

Department of Naval Architecture and Ocean Engineering, University of São Paulo, 05508-030 São Paulo, Brazil

ARTICLE INFO

Article history:
Received 2 February 2013
Received in revised form
30 May 2013
Accepted 3 June 2013

Keywords:
J-resistance curves
Ductile fracture
SE(T) specimen
SE(B) specimen
Crack growth

ABSTRACT

This work presents an investigation of the ductile tearing properties for a girth weld made of an API 5L X80 pipeline steel using experimentally measured crack growth resistance curves. Use of these materials is motivated by the increasing demand in the number of applications for manufacturing high strength pipes for the oil and gas industry including marine applications and steel catenary risers. Testing of the pipeline girth welds employed side-grooved, clamped SE(T) specimens and shallow crack bend SE(B) specimens with a weld centerline notch to determine the crack growth resistance curves based upon the unloading compliance (UC) method using the single specimen technique. Recently developed compliance functions and η-factors applicable for SE(T) and SE(B) fracture specimens with homogeneous material and overmatched welds are introduced to determine crack growth resistance data from laboratory measurements of load-displacement records.

1. Introduction

Structural integrity assessments of pipe girth welds play a key role in design and safe operation of piping systems, including deep water steel catenary risers. More efficient and faster installation methods now employ the pipe reeling process which allows welding and inspection to be conducted at onshore facilities (see, *e.g.*, [1,2]). The welded pipe is coiled around a large diameter reel on a vessel and then unreeled, straightened and finally deployed to the sea floor. However, the reeling process subjects the pipe to large bending loads and plastic deformation (2∼3%) well beyond the material's elastic limits with a potentially strong impact on flaw acceptance criteria for the girth weld. Consequently, accurate measurements of fracture resistance properties, including crack growth resistance curves of the girth weld material, become essential in defect assessment and fitness-for-service (FFS) procedures of the weldment region (which also includes the heat affected zone), where undetected crack-like defects (such as lack of penetration, deep undercuts, root cracks, etc.) may further extend due to the high tension stresses and strains imposed from the reeling process.

Fracture mechanics based approaches to describe ductile fracture behavior in structural components, including welded structures, rely upon crack growth resistance ($J-\Delta a$) curves (also often termed *R*-curves) to characterize crack extension followed by crack instability of the material [3,4]. In particular, FFS procedures applicable to reeled pipes [5] rely on direct applications of *J*-resistance data measured using small, laboratory fracture specimens to specify acceptable flaw sizes. These approaches allow the specification of critical crack sizes based on the predicted growth of crack-like defects under service conditions. Current standardization efforts now underway [6–9] advocate the use of single edge notch tension specimens (often termed SE(T) or SENT crack configurations) to measure experimental *R*-curves more applicable to high pressure piping systems and girth welds of marine steel risers.

The primary motivation to use SE(T) fracture specimens in defect assessment procedures for this category of structural components is the strong similarity in crack-tip stress and strain fields which drive the fracture process for both crack configurations [10–13]. Recent applications of SE(T) fracture specimens to characterize crack growth resistance properties in pipeline steels [14] have been effective in providing larger flaw tolerances while, at the same time, reducing the otherwise excessive conservatism which arises when measuring the material's fracture toughness based on high constraint, deeply-cracked, single edge notch bend SE(B) (also termed SENB crack configuration) or compact tension C(T) specimens. However, while now utilized effectively in fracture testing of pipeline girth welds,

* Corresponding author. Tel.: +55 1130915184; fax: +55 1130915717.
E-mail addresses: claudio.ruggieri@poli.usp.br, claudio.ruggieri@gmail.com (C. Ruggieri).

0308-0161/$ – see front matter © 2013 Elsevier Ltd. All rights reserved.
http://dx.doi.org/10.1016/j.ijpvp.2013.06.003

some difficulties associated with SE(T) testing procedures, including fixture and gripping conditions, raise potential concerns about the significance and qualification of measured crack growth resistance curves. Such uncertainties in measured fracture toughness may potentially affect tolerable defect sizes obtained from engineering critical assessment (ECA) procedures. While slightly more conservative, testing of shallow-crack bend specimens configuration may become more attractive due to its simpler testing protocol, laboratory procedures and much smaller loads required to propagate the crack. Although deeply-cracked SE(B) specimens are the preferred crack geometry often adopted in conventional defect assessment methods, recent revisions of ASTM 1820 [15] and ISO 15653 [16] have also included J-estimation equations applicable to shallow-crack bend specimens. Consequently, use of smaller specimens which yet guarantee adequate levels of crack-tip constraint to measure the material's fracture toughness becomes an attractive alternative.

This work presents an investigation of the ductile tearing properties for a girth weld made of an API 5L X80 pipeline steel using experimentally measured crack growth resistance curves (J–Δa curves). Use of these materials is motivated by the increasing demand in a number of applications for manufacturing high strength pipes for the oil and gas industry including marine applications and steel catenary risers. Testing of the pipeline girth welds employed side-grooved, clamped SE(T) specimens and shallow crack bend SE(B) specimens with a weld centerline notch to determine the crack growth resistance curves based upon the unloading compliance (UC) method using the single specimen technique. Recently developed compliance functions and η-factors applicable for SE(T) and SE(B) fracture specimens with homogeneous material and overmatched welds are introduced to determine crack growth resistance data from laboratory measurements of load-displacement records. This experimental characterization provides additional toughness data which serve to evaluate crack growth resistance properties of pipeline girth welds using SE(T) and SE(B) specimens with weld centerline cracks.

2. Overview of J-resistance curve measurements based on the UC procedure

Conventional testing programs to measure crack growth resistance (J–Δa) curves in metallic materials routinely employ the unloading compliance (UC) method based on a single specimen test. A key step in the experimental evaluation of the fracture resistance response for these specimens involves the estimation procedure for the J-integral as a function of applied (remote) loading and crack size. This section provides the essential features of the analytical framework needed to determine J and Δa for common fracture specimens, including the SE(T) and SE(B) configurations, from laboratory measurements of load-displacement records. Attention is directed to an incremental procedure to obtain estimates of J and crack length for an extending crack based on crack mouth opening displacement (CMOD) data.

2.1. Evaluation procedure of J

The procedure to estimate crack growth resistance data considers the elastic and plastic contributions to the strain energy for a cracked body under Mode I deformation [4,17] so that J can be conveniently defined in terms of its elastic component, J_e, and plastic component, J_p, as

$$J = J_e + J_p = \frac{K_I^2}{E'} + \frac{\eta A_p}{bB_N} \tag{1}$$

where K_I is the elastic stress intensity factor for the cracked configuration, A_p represents the plastic area under the load-displacement curve, B_N is the net specimen thickness at the side groove roots ($B_N = B$ if the specimen has no side grooves where B is the specimen gross thickness), b denotes the uncracked ligament ($b = W-a$ where W is the width of the cracked configuration and a is the crack length). In writing the first term of Eq. (1), plane-strain conditions are adopted such that $E' = E/(1-\nu^2)$ where E and ν are the (longitudinal) elastic modulus and Poisson's ratio, respectively.

Factor η appearing in the second term of Eq. (1) represents a nondimensional parameter which relates the plastic contribution to the strain energy for the cracked body with J. Fig. 1(a) illustrates the essential features of the estimation procedure for the plastic component J_p. Here, we note that A_p (and consequently, η_J) can be defined in terms of load–load line displacement (LLD or Δ) data or load-crack mouth opening displacement (CMOD or V) data. For definiteness, these quantities are denoted $\eta_{J-\mathrm{LLD}}$ and $\eta_{J-\mathrm{CMOD}}$.

The previous Eq. (1) defines the key quantities driving the evaluation procedure for J as a function of applied (remote) loading and crack size. However, the area under the actual load-displacement curve for a growing crack differs significantly from the corresponding area for a stationary crack (which the deformation definition of J is based on) [4,8,18]. Consequently, the measured load-displacement records must be corrected for crack extension to obtain accurate estimates of J-values with increased crack growth (see further details in Ref. [8]). A widely used approach (which forms the basis of current standards such as ASTM E1820 [15]) to evaluate J with crack extension follows from an incremental procedure which updates J_e and J_p at each partial unloading point, denoted k, during the measurement of the load vs. displacement curve illustrated in Fig. 1(b) as

$$J^k = J_e^k + J_p^k \tag{2}$$

where the current elastic term is simply given by

$$J_e^k = \left(\frac{K_I^2}{E'}\right)_k \tag{3}$$

For the SE(B) and C(T) configurations analyzed here, solutions for K_I can be found in several previously published works, such as Tada et al. [19], whereas Cravero and Ruggieri [7] provide K_I-solutions for clamped SE(T) specimens.

Evaluation of the plastic term, J_p^k, deserves further discussion. Early methods to measure J-resistance curves adopted an incremental equation to estimate J_p based entirely on load–load line displacement (LLD) records which derives from the fundamental work of Ernst et al. [18]. In addition to the η-factor introduced previously, the approach relies on a geometric γ-factor to correct the incremental plastic work for crack growth. Given the conditions of J-controlled crack growth and deformation plasticity are satisfied, the methodology enables approximate (but highly accurate) estimates of J_p for arbitrary (small) increments of crack length and load line displacement. However, when crack growth response is measured using load-crack mouth opening displacement (CMOD) records, direct application of Ernst's incremental formulation to evaluate J_p at each partial unloading point does not hold true. Recognizing this limitation, Cravero and Ruggieri [8] and Zhu et al. [20] introduced an incremental formulation to determine J_p which is more applicable to CMOD data in the form

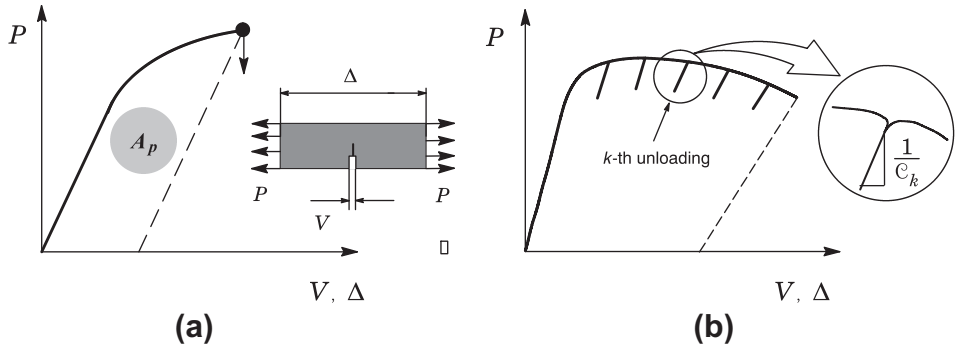

Fig.1. (a) Definition of the plastic area under the load-displacement curve; (b) Partial unloading during the evolution of load with displacement.

$$J_p^k = \left[J_p^{k-1} + \frac{\eta_{J-\mathrm{CMOD}}^{k-1}}{b_{k-1}B_N}\left(A_p^k - A_p^{k-1}\right)\right]\left[1 - \frac{\gamma_{\mathrm{LLD}}^{k-1}}{b_{k-1}}(a_k - a_{k-1})\right] \quad (4)$$

where factor γ_{LLD} is evaluated from

$$\gamma_{\mathrm{LLD}}^{k-1} = \left[-1 + \eta_{J-\mathrm{LLD}}^{k-1} - \left(\frac{b_{k-1}}{W\eta_{J-\mathrm{LLD}}^{k-1}}\frac{d\eta_{J-\mathrm{LLD}}^{k-1}}{d(a/W)}\right)\right] \quad (5)$$

The incremental expression for J_p defined by Eq. (4) contains two contributions: one is from the plastic work in terms of CMOD and, hence, $\eta_{J-\mathrm{CMOD}}$ and the other is due to crack growth correction in terms of LLD by means of $\eta_{J-\mathrm{LLD}}$. While the resulting J-estimation procedure based on CMOD may appear a little more complex, evaluation of Eq. (4) coupled with Eq. (5) is also relatively straightforward provided the two geometric factors, $\eta_{J-\mathrm{CMOD}}$ and $\eta_{J-\mathrm{LLD}}$, are known. Section 4 addresses crack growth resistance testing of fracture specimens with different geometries which include: 1) clamped SE(T) specimen; 2) conventional SE(B) specimen and 3) standard C(T) specimen. The corresponding η-factor equations are provided in the following subsections.

2.1.1. Clamped SE(T) specimens

Single edge-notched tension SE(T) specimens with fixed-grip loading have been increasingly used in crack growth resistance measurements for key structural applications, including girth weld defect assessments in oil and gas transmission pipelines and submarine risers. Because this specimen may be viewed as a nonstandard configuration, only a few previous studies [6,7,9,21–23] have developed wide range J estimation equations for SE(T) geometries based on η-factors. In related work, Cravero and Ruggieri [7] and Ruggieri [22] provide an extensive body of results covering $\eta_{J-\mathrm{CMOD}}$ and $\eta_{J-\mathrm{LLD}}$ values for different hardening properties and varying a/W and H/W range; here, a is the crack size, W denotes the specimen width and H is the clamp distance (refer to Fig. 2 next for the specimen geometry). To facilitate manipulation of their results while, at the same time, providing a more direct evaluation procedure, the functional dependence of the η-factor with crack size and clamp distance can be rewritten in simpler forms summarized as follows

$$\left[\eta_{J-\mathrm{CMOD}}^{\mathrm{SET}}\right]_{H/W=10} = 1.067 - 1.767\frac{a}{W} + 7.808\left(\frac{a}{W}\right)^2 - 18.269\left(\frac{a}{W}\right)^3 + 15.295\left(\frac{a}{W}\right)^4 - 3.083\left(\frac{a}{W}\right)^5 \quad (6)$$

$$\left[\eta_{J-\mathrm{LLD}}^{\mathrm{SET}}\right]_{H/W=10} = -0.623 + 9.336\frac{a}{W} - 4.584\left(\frac{a}{W}\right)^2 - 47.963\left(\frac{a}{W}\right)^3 + 87.697\left(\frac{a}{W}\right)^4 - 44.875\left(\frac{a}{W}\right)^5 \quad (7)$$

$$\left[\eta_{J-\mathrm{CMOD}}^{\mathrm{SET}}\right]_{H/W=6} = 1.081 - 2.219\frac{a}{W} + 11.897\left(\frac{a}{W}\right)^2 - 35.689\left(\frac{a}{W}\right)^3 + 46.633\left(\frac{a}{W}\right)^4 - 21.792\left(\frac{a}{W}\right)^5 \quad (8)$$

$$\left[\eta_{J-\mathrm{LLD}}^{\mathrm{SET}}\right]_{H/W=6} = -1.0267 + 19.906\frac{a}{W} - 72.889\left(\frac{a}{W}\right)^2 + 126.378\left(\frac{a}{W}\right)^3 - 107.534\left(\frac{a}{W}\right)^4 + 35.801\left(\frac{a}{W}\right)^5 \quad (9)$$

where it is understood that a 5-th order polynomial fitting valid in the range $0.2 \le a/W \le 0.7$ is employed. Appendix A compares the above η-factor equations with other J estimation equations for SE(T) geometries previously reported by DNV F-108 [6] and Shen and Tyson [9].

2.1.2. 3P SE(B) specimens

Research efforts to improve fracture toughness testing methods based on conventional SE(B) specimens (with $W/B = 2$ configuration) have recently introduced revised J-integral equations and improved η-factors [24–28]. Here, we use an appropriate polynomial fitting to describe the results provided by Donato and Ruggieri [26] which allows defining the η-factors for the SE(B) specimens as

$$\eta_{J-\mathrm{CMOD}}^{\mathrm{SEB}} = 3.650 - 2.111\frac{a}{W} + 0.341\left(\frac{a}{W}\right)^2 \quad (10)$$

and

$$\eta_{J-\mathrm{LLD}}^{\mathrm{SEB}} = 0.020 + 18.086\frac{a}{W} - 73.246\left(\frac{a}{W}\right)^2 + 152.225\left(\frac{a}{W}\right)^3 - 159.769\left(\frac{a}{W}\right)^4 + 66.879\left(\frac{a}{W}\right)^5 \quad (11)$$

which are valid in the range $0.1 \le a/W \le 0.7$. The above equations agree very well with the revised J-integral expressions developed by Zhu et al. [20] which form the basis of current ASTM E1820 [15] and ISO 15653 [16] standards using CMOD records.

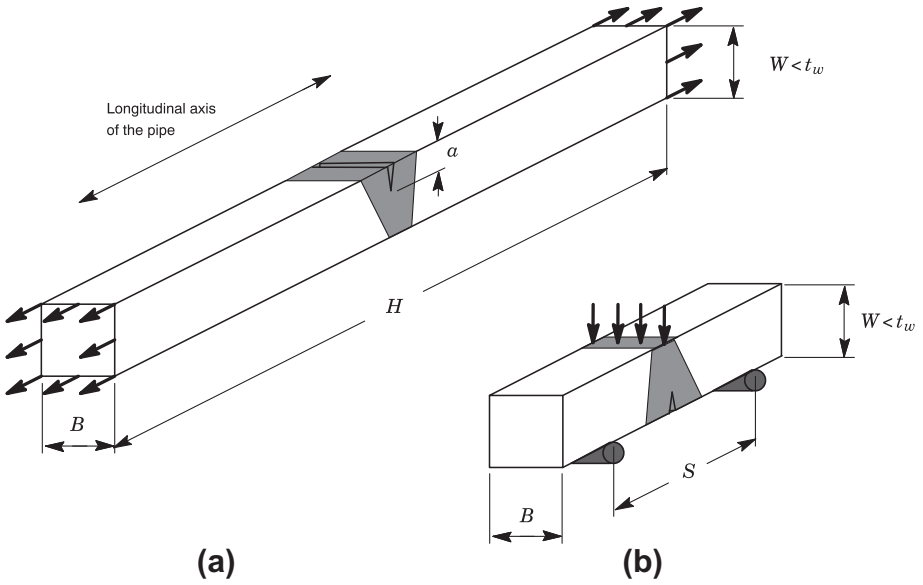

Fig. 2. Geometry of tested fracture specimens with weld centerline notch and $B \times B$ configuration: (a) Clamped SE(T) specimen with $a/W = 0.4$ and $H/W = 10$; (b) 3P SE(B) specimen with $a/W = 0.25$ and $S/W = 4$.

The previous η-factor equations reflect the effect of strain energy for the cracked body, described by the plastic work associated with the load-displacement curve (see Fig. 1), on the applied J derived from plane-strain analyses of conventional SE(B) specimens with $W/B = 2$. In related work, Nevalainen and Dodds [29] examined the through-thickness dependence of the crack front fields in 3-D models of SE(B) configurations to find a coupling effect of a/W and W/B ratios with material hardening properties on fracture behavior. In particular, they reported plastic η-factors for selected bend geometries with $W/B = 1$ that differ from the corresponding η-values for conventional bend specimens with $W/B = 2$ thereby affecting the experimentally measured values of J determined from the load-displacement records. Nevalainen and Dodds [29] attributed such differences to anticlastic bending effects which develop in the $W/B = 1$ configuration not present in bend geometries with larger W/B-ratios. To address this issue, Appendix B provides further developments in the J estimation procedure and associated η-factors applicable to SE(B) specimens with $W/B = 1$ configuration. Specifically, for the tested SE(B) geometry having $B = 14.8$ mm and width $W = 14.8$ mm (see Section 3), the η-factors derived from the 3-D analyses described in Appendix B are given by

$$\eta^{\mathrm{SEB}}_{J-\mathrm{CMOD}} = 3.341 - 1.907\frac{a}{W} - 0.641\left(\frac{a}{W}\right)^2 \tag{12}$$

$$\eta^{\mathrm{SEB}}_{J-\mathrm{LLD}} = 0.609 + 0.870\frac{a}{W} + 36.837\left(\frac{a}{W}\right)^2 - 152.332\left(\frac{a}{W}\right)^3 + 224.731\left(\frac{a}{W}\right)^4 - 116.765\left(\frac{a}{W}\right)^5 \tag{13}$$

which are valid in the range $0.1 \le a/W \le 0.7$. Appendix A also compares the η-factor equations for the SE(B) configuration adopted in the present work, including previous Eqs. (12) and (13), with the J estimation equations reported by other studies.

2.1.3. C(T) specimens

Early work to develop a single-specimen experimental procedure for laboratory measurements of J [30] focused on the utilization of compact tension C(T) specimens which still represent the predominant configuration in current standards to evaluate crack growth resistance behavior. However, ASTM E1820 [15] specifies a cut-out added to the standard C(T) geometry of the early ASTM E399 [31] thereby allowing measurement of the load line displacement as the crack mouth opening displacement. Consequently, the J-integral formulations, including the compliance equations to estimate crack length discussed next, given by ASTM E1820 [15] are valid only for LLD measurements. When the standard C(T) configuration is utilized and CMOD records are measured in the test procedure, additional equations defining the functional dependence of factor η with crack size are needed.

Here, we build upon recent work of Savioli and Ruggieri [32] to arrive at the following set of equations for the η-factors

$$\eta^{\mathrm{CT}}_{J-\mathrm{CMOD}} = -2.264 + 18.244\frac{a}{W} - 26.430\left(\frac{a}{W}\right)^2 + 12.124\left(\frac{a}{W}\right)^3 \tag{14}$$

and

$$\eta^{\mathrm{CT}}_{J-\mathrm{LLD}} = -1.699 + 19.807\frac{a}{W} - 30.118\left(\frac{a}{W}\right)^2 + 14.099\left(\frac{a}{W}\right)^3 \tag{15}$$

which are valid in the range $0.45 \le a/W \le 0.7$.

2.2. Experimental estimation of crack extension

Current testing protocols to measure the crack growth resistance response using a single-specimen test are primarily based on the unloading compliance (UC) technique to obtain accurate estimates of the (current) crack length from the specimen compliance measured at periodic unloadings with increased deformation. Fig. 1(b) illustrates the essential features of the method. The slope of the load-displacement curve during the k-th unloading defines the current specimen compliance, denoted C_k, which depends on specimen geometry and crack length. For the crack configurations analyzed here, the specimen compliance based on CMOD is most often defined in terms of normalized quantities expressed as

$$\mu_{CMOD}^{SET} = \left[1 + \sqrt{EB_eC_{CMOD}}\right]^{-1} \tag{16}$$

$$\mu_{CMOD}^{CT} = \left[1 + \sqrt{EB_eC_{CMOD}}\right]^{-1} \tag{17}$$

$$\mu_{CMOD}^{SEB} = \left[1 + \sqrt{\frac{EWB_eC_{CMOD}}{S/4}}\right]^{-1} \tag{18}$$

where μ_{CMOD}^{SET}, μ_{CMOD}^{CT} and μ_{CMOD}^{SEB} define the normalized compliances for the SE(T), C(T) and SE(B) specimens. In the above expressions, E is the longitudinal elastic modulus, C_{CMOD} denotes the specimen compliance defined in terms of crack mouth opening displacement ($C = V/P$ where V is the CMOD and P represents the applied load) and the effective thickness is defined by

$$B_e = B - \frac{(B - B_N)^2}{B} \tag{19}$$

By measuring the instantaneous compliance during unloading of the specimen illustrated in Fig. 1(b), the current crack length follows directly from solving the functional dependence of crack length and specimen compliance in terms of μ_{CMOD}. For the clamped SE(T) specimen analyzed here, Cravero and Ruggieri [7] provides results for μ_{CMOD}^{SET} as

$$\left[\frac{a}{W}\right]_{H/W=10}^{SET} = 1.9215 - 13.2195\mu + 58.7080\mu^2 - 155.2823\mu^3 + 207.3987\mu^4 - 107.9176\mu^5 \tag{20}$$

and

$$\left[\frac{a}{W}\right]_{H/W=6}^{SET} = 2.1509 - 13.2405\mu + 48.8649\mu^2 - 110.8908\mu^3 + 131.1808\mu^4 - 61.2957\mu^5 \tag{21}$$

which are valid in the range $0.1 \le a/W \le 0.7$.

For the SE(B) specimen, the present work adopts the shallow-crack compliance expression provided by current ASTM 1820 [15] standard in the form

$$\left[\frac{a}{W}\right]_{S/W=4}^{SEB} = 1.01878 - 4.5367\mu + 9.0101\mu^2 - 27.333\mu^3 + 74.4\mu^4 - 71.489\mu^5 \tag{22}$$

where a/W ranges from 0.05 to 0.45. The above equation agrees well with the elastic compliance for the three-point bend configuration given by Tada et al. [19]. Moreover, as described in Appendix A, Eq. (22) is essentially identical to the elastic compliance derived from 3-D elastic analyses for SE(B) specimens with $W/B = 1$ and $0.1 \le a/W \le 0.7$ as well as to the deep crack compliance also given by ASTM 1820 [15].

We now direct attention to the unloading compliance testing of the C(T) specimen. As already noted, the compliance equations to estimate crack length given by ASTM 1820 [15] are applicable to LLD measurements only. Use of the standard C(T) configuration requires an additional compliance equation to estimate the crack length from CMOD measurements which is provided by Ruggieri [33] as

$$\left[\frac{a}{W}\right]^{CT} = 0.9368 - 2.1607\mu - 19.3666\mu^2 + 57.5279\mu^3 \tag{23}$$

with $0.40 \le a/W \le 0.7$. Again, the above equation agrees very well with the elastic compliance for the compact tension configuration given by Tada et al. [19].

2.3. Effects of weld strength overmatch on plastic η-factors

Current test standards employ J estimation expressions which are mainly applicable to fracture specimens made of homogeneous materials. For a given specimen geometry, mismatch between the weld metal and base plate strength affects the macroscopic mechanical behavior of the specimen in terms of its load-displacement response with a potentially strong impact on the coupling relationship between J and the near-tip stress fields. Accurate estimation formulas for J more applicable to welded fracture specimens may become important in robust defect assessment procedure capable of including effects of weld strength mismatch on the measured fracture toughness.

By defining the mismatch ratio, M_y, as

$$M_y = \frac{\sigma_{ys}^{WM}}{\sigma_{ys}^{BM}} \tag{24}$$

where σ_{ys}^{BM} and σ_{ys}^{WM} denote the yield stress for the base plate and weld metal, we build upon previous work of Donato et al. [34], Paredes and Ruggieri [23] and Savioli and Ruggieri [32] to introduce a functional dependence of factor η_{J-CMOD} with crack size and strength mismatch level for the tested fracture specimens which are summarized as follows

$$\eta_{J-CMOD}^{SEB} = 3.882 + 0.222\frac{a}{W} - 5.012\left(\frac{a}{W}\right)^2 + 4.021\left(\frac{a}{W}\right)^3 - 0.407M_y - 0.050M_y^2 \tag{25}$$

which is valid in the range $0.1 \le a/W \le 0.7$ and $1.0 < M_y \le 1.5$ [34],

$$\eta_{J-CMOD}^{SET} = -0.356 + 11.686\frac{a}{W} - 23.589\left(\frac{a}{W}\right)^2 + 13.899\left(\frac{a}{W}\right)^3 - 0.276M_y - 0.034M_y^2 \tag{26}$$

where a/W ranges between 0.2 and 0.7 and $1.0 < M_y \le 1.5$ [23] and

$$\eta_{J-CMOD}^{CT} = -3.864 + 29.086\frac{a}{W} - 46.404\left(\frac{a}{W}\right)^2 + 24.415\left(\frac{a}{W}\right)^3 - 0.252M_y - 0.106M_y^2 \tag{27}$$

which is valid in the range $0.45 \le a/W \le 0.7$ and $1.0 < M_y \le 1.5$ [32].

3. Experimental program

3.1. Material description and welding procedure

The material utilized in this study was a high strength, low alloy (HSLA), API grade X80 pipeline steel produced as a base plate using a control-rolled processing route without accelerated cooling. The mechanical properties and strength/toughness combination for this material are mainly obtained by both grain size refinement and second-phase strengthening due to the small-size precipitates in the matrix. The 20-inch pipe with longitudinal seam weld from which the girth weld SE(T), SE(B) and C(T) specimens were extracted was fabricated using the UOE process.

The tested weld joint was made from the API X80 UOE pipe having thickness, $t_w = 19$ mm. Girth welding of the pipe was performed using

the FCAW process in the 1G (flat) position with a single V-groove configuration in which the root pass was made by GMAW welding. The main weld parameters used for preparation of the test weld using the FCAW process are: i) number of passes 12 (including the root pass made by the GMAW process); ii) welding current 165 A; iii) welding voltage 23 V; iv) average heat input 1.5 kJ/mm.

3.2. Specimen geometries

Unloading compliance (UC) tests at room temperature were performed on weld centerline notched SE(T) specimens with fixed-grip loading to measure tearing resistance curves in terms of $J-\Delta a$ data. The clamped SE(T) specimens illustrated in Fig. 2(a) have a fixed overall geometry and crack length to width ratio defined by $a/W = 0.4$, $H/W = 6,10$ with thickness $B = 14.8$ mm, width $W = 14.8$ mm and clamp distance $H = 88.8$ and 148 mm. Here, a is the crack depth and W is the specimen width which is slightly smaller than the pipe thickness, t_w. Because the level of crack-tip constraint in clamped SE(T) specimens is weakly dependent on crack size (as characterized by the a/W-ratio) [11], the tested SE(T) geometry with $a/W = 0.4$ represents fairly well the crack resistance behavior for this crack configuration having other a/W-ratios. Indeed, DNV F108 [6] allows testing of clamped SE(T) specimens with any crack size over specimen width ratio as long as $0.2 \leq a/W \leq 0.5$.

UC tests at room temperature were also conducted on weld centerline notched SE(B) specimens shown in Fig. 2(b) with $a/W = 0.25$ with thickness $B = 14.8$ mm, width $W = 14.8$ mm and span $S = 4W$. Additional fracture tests were performed on deeply-cracked C(T) specimens having standard geometry with $a/W = 0.5$, thickness $B = 14.0$ mm and width $W = 56.0$ mm; testing of this crack configuration provides a baseline J-resistance curve against which ductile tearing behavior for other crack configurations can be compared. Conducted as part of a collaborative research program at University of São Paulo on structural integrity assessment of marine steel catenary risers (SCRs), testing of these specimens focused on the development of accurate procedures to evaluate crack growth resistance data for pipeline girth welds.

The SE(B) and C(T) specimens were precracked using conventional techniques as recommended in ASTM E1820 [15]. The SE(T) configuration was precracked in bending using a three-point bend apparatus very similar to a conventional three-point bend test. After fatigue precracking, the specimens were side-grooved to a net thickness of ~85% the overall thickness (7.5% side-groove on each side with a 0.5 mm side-groove root radius) to promote uniform crack growth and tested following some general guidelines described in ASTM E1820 standard [15]. Records of load vs. crack mouth opening displacements (CMOD) were obtained from the specimens using a clip gauge mounted on knife edges attached to the specimen surface.

4. Crack growth resistance results

The following sections provide key results of the crack growth resistance testing conducted on fracture specimens extracted from the pipe girth weld. Primary attention is given to the effects of geometry and loading mode on J-resistance curves. The presentation considers measured experimental data directly associated with crack configurations which are now routinely adopted in current defect assessment procedures for pipelines and similar structural components. Although a number of previous studies favor the utilization of clamped SE(T) specimens, systematic studies that compare the toughness measuring capacity of this geometry with fracture resistance behavior of the SE(B) specimen remain relatively rare. Consequently, experimental analyses to verify the overall capability of both configurations to describe ductile fracture response provide further insight and an additional case for the use of shallow-crack bend specimens.

4.1. Mechanical properties of tested welds

Mechanical tensile tests, conducted on longitudinal tensile specimens (ASTM E8), provide the room temperature (20 °C) stress–strain data for the materials. Because of the pipe thickness and pipe curvature, subsized test specimens (6.5 mm gage diameter) for both base plate and weldment were utilized. The tensile specimens for the weld metal were machined from the weld fusion zone with their longitudinal axes parallel to the welding direction. Fig. 3 shows the engineering stress–strain curves for the base plate and weldment from which the following average tensile properties are defined: $\sigma_{ys}^{BM} = 609$ MPa and $\sigma_{uts}^{BM} = 679$ MPa; $\sigma_{ys}^{WM} = 716$ MPa and $\sigma_{uts}^{WM} = 750$ MPa. Based on Annex F of API 579 [35], the Ramberg-Osgood strain hardening exponents describing the stress–strain response for the base plate and weld metal are estimated as $n_{BM} = 20.3$ and $n_{WM} = 35.2$. The measured tensile properties indicate that the weldment overmatches the base plate material by 18% ($M_y = 1.18$ – refer to Eq. (24) for definition of the mismatch level) at room temperature.

4.2. J-resistance curves

The framework for determining J-resistance curves based on CMOD from conventional fracture specimens, including the SE(T) configuration, described in previous Section 2 provides the basis for evaluating ductile fracture response of the tested material while, at the same time, assessing effects of specimen geometry and loading mode on the $J-\Delta a$ data. We first draw attention to the load carrying capacity for the bend and tension configurations. Fig. 4 shows a typical load-

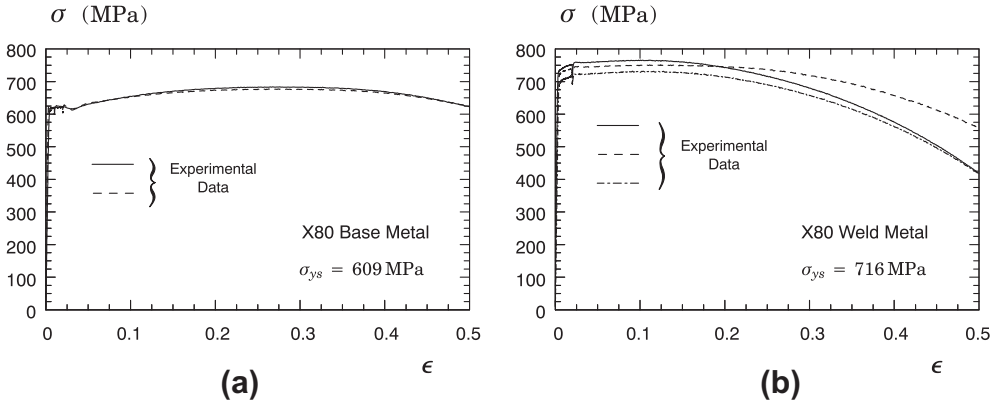

Fig. 3. Tensile data for the tested X80 pipeline steel at room temperature: (a) Base plate material; (b) Weldment.

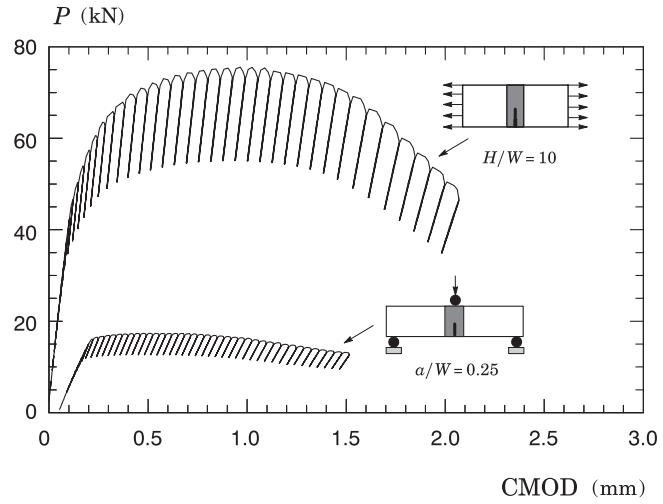

Fig. 4. Measured load-CMOD curve for the tested X80 pipeline girth weld using clamped SE(T) specimens with $a/W = 0.4$ and 3P SE(B) specimens with $a/W = 0.25$.

displacement curve (as described by CMOD) measured from testing the SE(T) specimen with $H/W = 10$, $a/W = 0.4$ and the shallow crack SE(B) configuration with $a/W = 0.25$. The strong effect of loading mode (tension *vs.* bending) associated with specimen geometry is evident in this plot. At similar levels of crack mouth opening displacement, the applied load for the SE(T) specimen increases approximately by a factor of 4 compared to the load response for the SE(B) specimen.

Figs. 5–10 show the measured resistance curves for the tested crack configurations with different specimen geometries and a/W-ratios. Consider first the effect of crack growth correction on the resistance curves for the SE(T) specimen with $H/W = 10$ displayed in Fig. 5 (with no crack growth correction) and 6 (which incorporates crack growth correction). These two sets of curves show that crack growth correction lowers the measured fracture resistance for a given Δa-value, particularly for increased crack extension. Here, the fracture resistance measured in terms of J for the results with crack growth correction shown in Fig. 6 is reduced by 10 ~ 15% for $\Delta a \geq 2$ mm compared to the results displayed in Fig. 5; such behavior is in accord with previous findings by Cravero and Ruggieri [8]. Very similar trends are observed for the measured resistance curves obtained from other fracture specimens. Since the focus here lies on comparisons of J–Δa response for different crack configurations, the results described subsequently are derived from using the crack growth correction term to determine J – see Eq. (4).

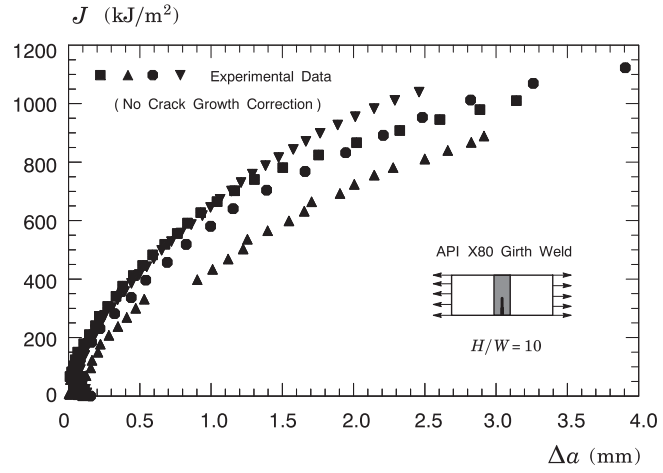

Fig. 5. J-resistance curves without crack growth correction for the tested clamped SE(T) specimens with $a/W = 0.4$ and $H/W = 10$.

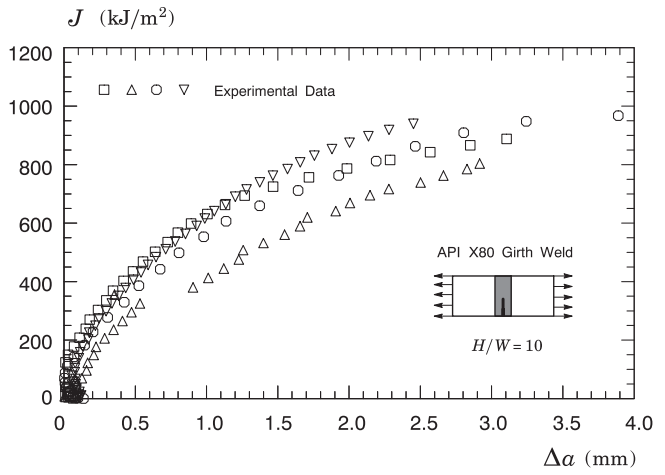

Fig. 6. J-resistance curves including crack growth correction for the tested clamped SE(T) specimens with $a/W = 0.4$ and $H/W = 10$.

Fig. 7 displays the J-resistance curves for the SE(T) specimen with $H/W = 6$. It is seen that the measured crack growth response for this configuration is essentially similar to the previous resistance curves for the SE(T) specimen with $H/W = 10$ shown in Fig. 6. It is evident the little influence of the clamp distance, H, on the J–R curves for this specimen configuration within the tested H/W range. A small effect of the H/W-ratio on the average slope (which is interpreted as the material's tearing modulus [4]) of the resistance curves is noticed with slightly higher tearing modulus observed in the experimental data for the configuration with $H/W = 6$. Further, we also note that the average J-values at a fixed amount of crack growth, $\Delta a = 1$ mm, for the SE(T) specimen with $H/W = 10$ are slightly higher than the corresponding J-values for the SE(T) configuration with $H/W = 6$. However, such differences can be considered minimal since all resistance curves lie within the inherent material variability of the measured data band.

Now direct attention to the crack growth response for the shallow crack SE(B) specimens with $W/B = 1$ shown in Figs. 8 and 9. Here, we provide J–Δa data for this crack configuration based on η-factors defined by Eqs. (10) and (11), which derive from plane-strain analyses of a $W/B = 2$ geometry (see Fig. 8), and on η-factors from the 3-D analyses given by Eqs. (12) and (13) as described in Appendix B (see Fig. 9). Clearly, the adopted procedure to evaluate the plastic component J_p (using either of the previous expressions for factors $\eta_{J-\mathrm{CMOD}}$ and $\eta_{J-\mathrm{LLD}}$) has a rather pronounced effect on the

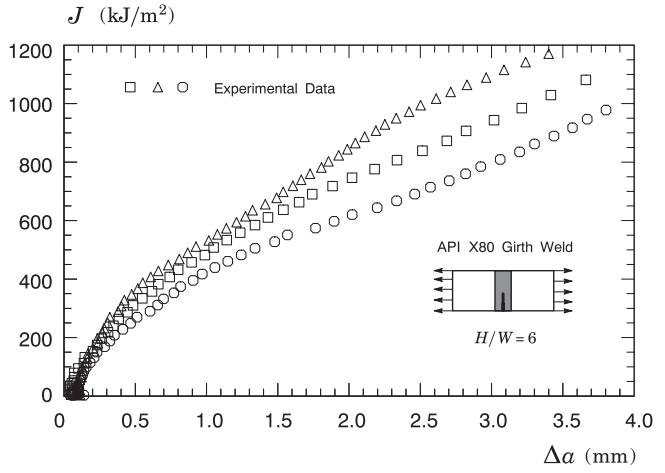

Fig. 7. J-resistance curves including crack growth correction for the tested clamped SE(T) specimens with $a/W = 0.4$ and $H/W = 6$.

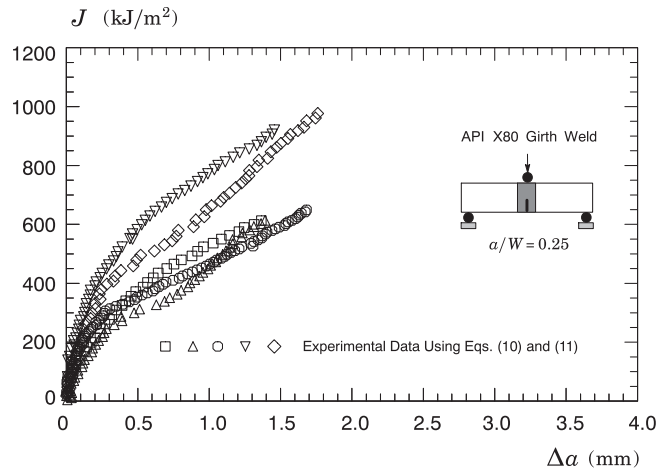

Fig. 8. *J*-resistance curves including crack growth correction for the tested SE(B) specimens with $a/W = 0.25$ and $W/B = 1$ using η-factors from Eqs. (10) and (11).

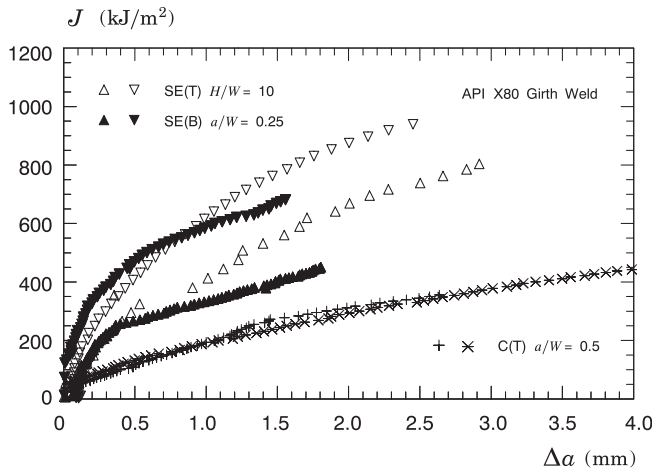

Fig. 10. Comparison of *J*-resistance curves including crack growth correction for different specimen geometries.

measured *J*-resistance curves. Observe that, because the plane-strain and 3-D elastic compliance for this specimen geometry are virtually identical (see Appendix A), such differences in the resistance curves can be entirely attributed to the effect of factor η on the J_p-value. Further observe that the higher (nonconservative) $J-\Delta a$ response in Fig. 8 is based on Eqs. (10) and (11) which yield essentially the same η-factors provided by current ASTM E1820 [15] and ISO 15653 [16] standards. These differences in $J-R$ curves for the tested SE(B) specimens with $W/B = 1$ exhibited in Figs. (8) and (9) appear sufficiently large to raise concerns in testing procedures utilizing square cross section bend specimens to measure crack growth resistance behavior based on current standard formulations.

Moreover, a particularly salient feature associated with these previous results is that the fracture resistance values for the shallow crack SE(B) configuration are relatively similar (albeit somewhat smaller) to the corresponding values in Figs. 6 and 7 for the SE(T) specimens. Unfortunately, the measured resistance curves are perhaps somewhat more scattered that we would expect for these specimens. Part of such scatter can be attributed to the differences in the initial (measured) precrack sizes which result in actual a/W-ratios ranging from 0.25 to 0.34 for this crack configuration (refer to Table 1) – note that crack-tip constraint for the SE(B) specimen exhibits rather strong sensitivity to crack size which also impacts crack growth resistance values. While we did not investigate thoroughly such behavior, the crack front measurements addressed later in Section 4.4 reveal a rather highly uneven crack advance, thus providing some explanation for the shape of the measured resistance curves. However, it is nevertheless evident that the *J*-resistance data for the SE(B) configuration compare relatively well with the SE(T) specimen results, particularly when the η-factors from the 3-D analyses described in Appendix B are incorporated into the *J* evaluation procedure.

Fig. 10 provides a summary plot which emphasizes the effect of specimen geometry on the crack growth resistance behavior for the tested API X80 girth weld. The plot also includes the measured resistance curves for the C(T) specimen with $a/W = 0.5$; this crack configuration has the highest crack-tip constraint thereby producing the lowest $J-\Delta a$ response. To facilitate comparison, only the lowest and highest resistance curves for the shallow crack SE(B) specimen and SE(T) configuration with $H/W = 10$ are included in the plot; these curves can therefore be interpreted as the measured data band for these specimens. As already observed, an evident feature emerging from these results is that there appears to be little geometry dependence of the *J*-resistance curves for the shallow crack SE(B) and SE(T) specimens. Here, the approximate average $J-R$ curve for the shallow crack SE(B) specimen is slightly lower than the corresponding average $J-\Delta a$ response for the SE(T) configuration. This result, however, should not be uncritically endorsed since, as discussed previously, the crack growth resistance data for the SE(B) specimen exhibited larger scatter associated with uneven crack advance which may diminish a little the rigor of the comparison. Further, there is a striking difference between the *J*-resistance curves for the deeply-cracked C(T) specimens and the SE(B) and SE(T) configurations, a behavior that was already anticipated. It can be reasonably concluded from the results displayed in this plot that, while the C(T) specimen provides very low *J*-resistance curves, crack growth response is likely to be sufficiently describable by either the shallow crack SE(B) specimen and the SE(T) specimen to serve as a basis for ductile tearing assessments in ECA procedures applicable to pipeline girth welds and similar structural components. In the present case, the SE(B) specimen would provide a somewhat more conservative assessment associated with its lower crack growth resistance curve.

Comparisons of the *J*-resistance curves for the clamped SE(T) configurations having $H/W = 10$ with previously developed procedure [9] for testing clamped SE(T) specimens further demonstrate the applicability of the estimation method for obtaining fracture resistance data presented here. Fig. 11 compares the *J*-resistance curves for the SE(T) specimen with $H/W = 10$ derived from using the estimation equations provided in previous Section 2.1.1 and the fracture resistance data based on the procedure recently developed by Shen and

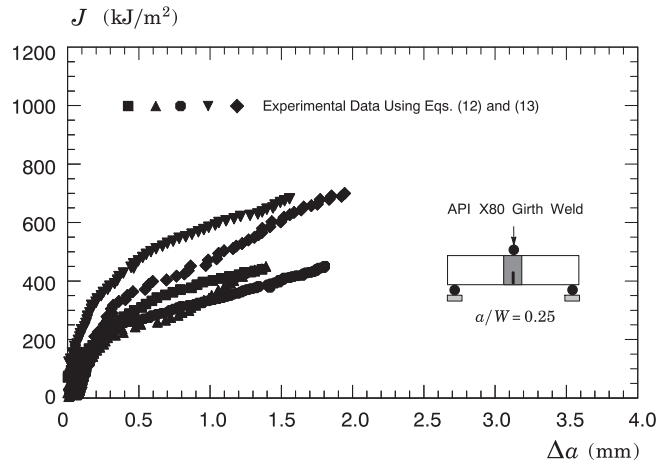

Fig. 9. *J*-resistance curves including crack growth correction for the tested SE(B) specimens with $a/W = 0.25$ and $W/B = 1$ using η-factors from Eqs. (12) and (13).

Table 1
Predicted and measured crack extension for all tested fracture specimens.

Specimen	Configuration	Compliance estimation			Measured post test		Deviation (%)
		a_0 (mm)	a_f (mm)	Δa (mm)	a_f (mm)	Δa (mm)	
SET1 H10	SE(T) $H/W = 10$	5.66	8.79	3.13	8.77	3.11	0.78
SET2 H10	SE(T) $H/W = 10$	6.11	8.66	2.55	8.56	2.45	3.87
SET3 H10	SE(T) $H/W = 10$	6.29	9.32	3.03	9.20	2.92	3.75
SET4 H10	SE(T) $H/W = 10$	6.70	10.59	3.89	10.59	3.89	0.03
SET1 H6	SE(T) $H/W = 6$	6.90	10.39	3.49	10.56	3.66	−4.90
SET2 H6	SE(T) $H/W = 6$	6.64	10.16	3.52	10.19	3.55	−0.73
SET3 H6	SE(T) $H/W = 6$	6.26	10.13	3.87	10.06	3.80	1.74
SEB1	SE(B) $a/W = 0.25$	4.38	6.28	1.90	5.89	1.39	26.84
SEB2	SE(B) $a/W = 0.25$	4.99	7.00	2.01	6.38	1.48	26.37
SEB3	SE(B) $a/W = 0.25$	4.48	6.65	2.17	6.12	1.78	17.88
SEB4	SE(B) $a/W = 0.25$	3.75	6.50	2.75	5.84	1.94	29.45
SEB5	SE(B) $a/W = 0.25$	3.93	6.25	2.32	5.30	1.65	28.88
CT1	C(T) $a/W = 0.5$	28.21	30.85	2.64	28.64	2.64	0.13
CT2	C(T) $a/W = 0.5$	27.60	34.16	6.56	34.54	7.04	−7.36

Tyson (S&T) [9]. To facilitate comparison, only selected resistance curves for the SE(T) configuration with $H/W = 10$ are included in the plot. While the overall trend of increased J-values with increased amount of ductile tearing is similar, the procedure developed in Ref. [9] produces somewhat higher resistance curves compared to the present results; here, differences are in the range of 20% for crack extension levels of ~2 mm. We also observe that, even though our η-factors and the results developed by S&T differ by less than 10%, differences in J are cumulative over the several unload steps during the incremental procedure until test termination. Appendix A compares the η-factor equations utilized in the present work with the J estimation equations for SE(T) geometries developed by Shen and Tyson [9].

4.3. Effects of weld strength overmatch on J–R curves

This section examines the effect of weld strength mismatch on the fracture resistance as measured by the J–Δa response for the tested SE(T) and SE(B) specimens with weld centerline notch. The primary objective is to gain further insight into the potential deviation that arises from evaluating the J-resistance curves using η-factors equations developed for homogeneous materials.

Fig. 12 compares the J-resistance curves for the shallow crack SE(B) specimen and SE(T) configuration with $H/W = 10$ based on η-factors for homogeneous materials and overmatched welds as represented by open and solid symbols. The η-values for the overmatch condition are determined from using the estimation equations provided in Section 2.3 with $M_y = 1.18$. Since the primary objective here is the assessment of weld strength mismatch on crack growth resistance behavior, these η-expressions derive from plane-strain analyses such that the J–Δa response for the SE(B) specimen with $W/B = 1$ is recast from previous Fig. 8. Again, to facilitate comparison, only the lowest and highest resistance curves for these crack configurations are included in the plot. The trend is clear. The fracture resistance curves derived from η-factors for overmatched welds are practically indistinguishable from the curves evaluated with η-factors for homogeneous materials. Here, use of η-factors for homogeneous materials (*i.e.*, not taking into account the degree of weld strength overmatch) leads to slightly nonconservative (higher) estimates of the resistance curve (we should emphasize that the larger the levels of weld strength mismatch the larger the degree of nonconservativeness).

4.4. Crack length measurements

Validation analyses of crack length estimates prove essential to assess the accuracy of the UC procedure to determine crack growth during the fracture test. Following standard methods based on the 9-point average technique, such as the procedure given by ASTM E1820 [15], the initial and final crack length measured after the test by means of an optical method are compared with crack length estimates derived from the UC method. Table 1 provides the predicted and measured crack extension for all tested fracture specimens in which the error (deviation) between predicted and measured values is defined as $(\Delta a_{\text{measured}} - \Delta a_{\text{predicted}})/\Delta a_{\text{measured}}$. The significant features that emerge from these results include: (1)

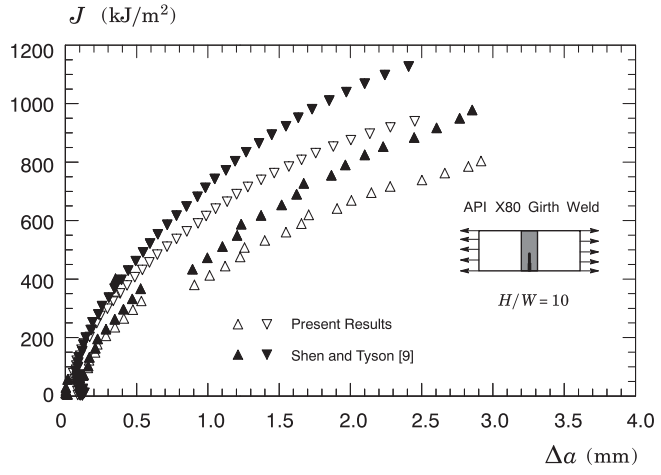

Fig. 11. Comparison of J-resistance curves for the SE(T) specimens with $H/W = 10$ based on the framework developed here and the procedure proposed by Shen and Tyson [9].

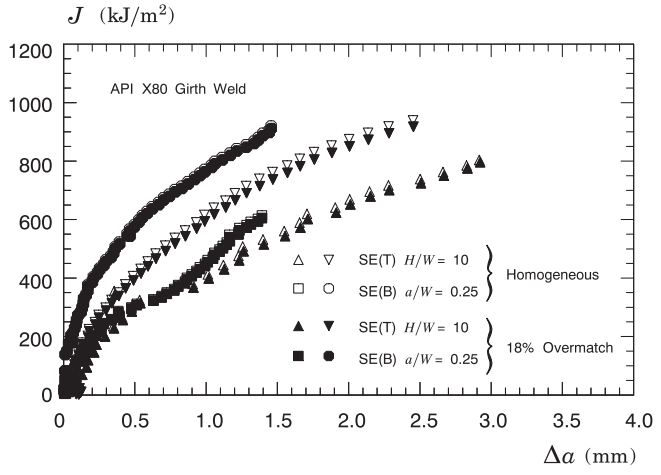

Fig. 12. J-resistance curves for tested clamped SE(T) specimen and shallow crack SE(B) specimen based upon η-factors for homogeneous materials and overmatched welds.

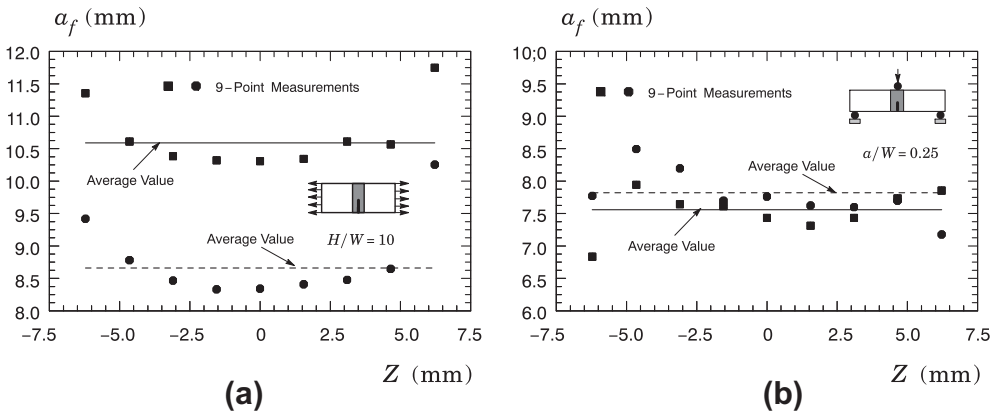

Fig. 13. Distribution of the measured final crack length, a_f, along the crack front for representative crack configurations: (a) SE(T) specimen with $H/W = 10$; (b) SE(B) specimen with $a/W = 0.25$.

predictions of crack extension based on the UC procedure for the SE(T) specimens are in close agreement with experimental measurements with a level of accuracy of ±5%; (2) crack growth estimates for the C(T) specimen by unloading compliance also display nearly the same accuracy as the SE(T) specimens; (3) crack extension predictions for the shallow crack SE(B) configuration derived from the UC procedure are not in good agreement with the measured amount of ductile tearing; here, the unloading compliance method underestimates the 9-point average crack extension by 25∼30% which produces apparent higher J-resistance curves.

This last feature deserves further discussion. The UC procedure described previously to estimate the current crack length involves the assumption of a straight crack front. Consequently, the compliance equations discussed in Section 2.2 (also Appendix A and B) should be viewed as idealized solutions providing estimates for the average crack extension. To a certain degree, the crack growth behavior for the shallow crack SE(B) configuration can be explained in terms of the uneven crack advance and a rather irregular crack front profile observed in these specimens. Moreover, further examination revealed that the bend specimens exhibited a highly non-uniform fatigue precrack compared to the SE(T) specimens; such feature could be caused by unexpected misalignment between the specimen and the rollers, affecting the crack tip stresses and strains driving the ductile fracture process.

To illustrate this issue, Fig. 13 shows the distribution of the measured final crack length, a_f, along the crack front ($Z = 0$ marks the center of specimen thickness) of two representative fracture specimens for the SE(T) and SE(B) configurations. In these plots, the solid symbols denote the 9-point experimental measurements and the corresponding average values are defined by dashed and solid lines. With exception of measured points lying near the side-groove ($Z = \pm 6.25$ mm), it can be seen that the SE(T) specimen displays a rather more uniform crack extension than the SE(B) specimen (notice that the scales are the same in the plots). Moreover, and perhaps more importantly, the inaccurate estimate of crack extension resulting from these analyses is suggestive of a strong effect of the bend loading mode on crack length predictions. Indeed, previous studies [36,37] have already indicated that use of the UC method with three-point bend specimens underestimates crack extension when compared with optically measured values of crack length; this effect appears to be more pronounced for SE(B) configurations with reduced size such as the bend specimen geometry used in the present work.

In related work on the effect of crack depth and mode of loading on J–R curve behavior, Joyce et al. [21] examined the crack growth response for a high strength steel using SE(B), SE(T) and double edge notch tension DE(T) specimens. They have also reported large differences (up to ∼35%) between UC predictions of crack extension and measured post test crack growth in nonside-grooved SE(B) specimens with smaller differences (up to ∼14%) in side-grooved specimens. Joyce et al. [21] also raised some concerns on the application of the UC procedure to estimate crack extension in bend specimens, particularly for nonside-grooved configurations. Currently, we consider this issue not fully resolved but provisionally accept the relatively good correlation thus established between the J-resistance curves for the shallow crack SE(B) specimens and clamped SE(T) configurations. Further analyses and additional experimental data are needed to support a more definite conclusion - an investigation along this line is in progress.

5. Concluding remarks

This study describes an experimental investigation of the ductile tearing properties for a girth weld made of an API 5L X80 pipeline steel using experimentally measured crack growth resistance curves (J–Δa curves). Testing of the pipeline girth welds utilized side-grooved, clamped SE(T) specimens and shallow crack bend SE(B) specimens with a weld centerline notch to determine the crack growth resistance curves based upon the unloading compliance (UC) method using a single specimen technique. This experimental characterization provides additional toughness data which serve to evaluate crack growth resistance properties of pipeline girth welds using SE(T) and SE(B) specimens with weld centerline cracks. The work described here supports the following conclusions:

1. Shallow-crack SE(B) specimens provide crack growth resistance curves which are somewhat lower than the J-resistance curves for clamped SE(T) specimens thereby yielding slightly more conservative crack growth resistance curves. While the relatively larger scatter of the J–Δa data and larger uncertainties in crack extension estimates for the shallow crack SE(B) configuration unfortunately preclude drawing a definite conclusion, the crack growth resistance behavior for this specimen geometry displays a clear trend of producing relatively similar (albeit smaller) J-resistance curve compared to the clamped SE(T) specimen;
2. There is little influence of the clamp distance, H, on the J–R curves for the clamped SE(T) specimen configuration within the tested H/W range. The analyses and test results show that the SE(T) specimen with $H/W = 10$ yields J-resistance curves that are slightly less conservative (slightly higher J–R curve) than the SE(T) configuration with $H/W = 6$;
3. Levels of weld strength overmatch within the range of 10∼20% overmatch do not affect significantly J-resistance curves derived from using η-values applicable to homogeneous materials. While the fracture resistance curves based on η-values for homogeneous materials are slightly higher than the corresponding

curves based on η-factors for overmatched weldments, differences are nevertheless small and within acceptable limits;
4. The plastic η-factors for SE(B) specimens with square cross section ($W/B = 1$) derived from 3-D analyses are significantly lower than the corresponding η-factors derived from plane-strain analyses of the preferred geometry ($W/B = 2$) thereby producing lower experimentally measured J-values;
5. Crack extension predictions based on the UC procedure agree well with experimental measurements for the SE(T) and C(T) specimens. In contrast, the unloading compliance method underestimates the 9-point average crack extension for the shallow crack SE(B) specimen by 25 ~ 30%. This rather strong underprediction of crack extension for this crack configuration produces apparent higher J-resistance curves while nevertheless allowing reasonable comparison of fracture resistance behavior across the tested specimen geometries.

While the analyses and test results described here provide an additional support to the use of shallow crack bend specimens as an alternative fracture specimen to measure crack growth properties for pipeline girth welds and similar structural components, they are also suggestive of the need for more experimental studies to validate the UC-based procedure for estimating J-resistance curves of SE(B) configurations. In particular, the larger uncertainties in crack extension estimates for this crack configuration underlie some potential difficulties that may have arisen during testing of a small size bend specimen, including achieving a straight and more even crack extension – this issue appears central to develop a more robust and efficient J-resistance evaluation procedure. Additional work is in progress along these lines of investigation covering crack growth resistance testing of an API X65 steel using SE(T) and SE(B) fracture specimens with varying a/W-ratios.

Acknowledgments

This investigation is primarily supported by Fundação de Amparo à Pesquisa do Estado de São Paulo (FAPESP) through Grant 2009/54229-3 and by Agência Nacional de Petróleo, Gás Natural e Biocombustíveis (ANP). The work of CR is also supported by the Brazilian Council for Scientific and Technological Development (CNPq) through Grants 304132/2009-8 and 476581/2009-5. The authors acknowledge Tenaris-Confab Brasil and Lincoln Electric Brasil for providing support for the experiments described in this work. Helpful comments by a reviewer are gratefully acknowledged.

A. Comparison of η-factor and elastic compliance equations for SE(T) and SE(B) specimens

Development of testing standards incorporating improved J and crack growth estimation equations for conventional fracture specimens has received considerable attention in recent years. The primary motivation driving these research efforts is the need of increased accuracy in fracture toughness measurements while, at the same time, allowing testing of a wider range of crack geometries such as the shallow crack SE(B) specimen and clamped SE(T) configuration. Here, we provide a comparison between the η-factor and elastic compliance equations adopted in the present work with other key related studies.

A.1. Clamped SE(T) specimens

While the clamped SE(T) specimen has been increasingly utilized as an alternative for the SE(B) configuration in integrity assessment procedures of pipeline girth welds subjected to plastic strains, it is currently considered a nonstandard geometry. Consequently, only limited results for η-factor and elastic compliance equations are available, including previous work of DNV F108 [6] and Shen and Tyson (S&T) [9] (however, DNV F108 adopts a multispecimen technique procedure and therefore does not provide elastic compliance equations).

Fig. 14(a–b) compares the $\eta_{J-\mathrm{CMOD}}$ and $\eta_{J-\mathrm{LLD}}$ equations adopted in this work with the η-results provided by DNV F108 [6] and S&T [9] for clamped SE(T) specimens with $H/W = 10$ and $W/B = 1$; this last guideline also includes a 0.85 reduction factor in the η-values for added conservatism. Moreover, because DNV F108 procedure limits the amount of ductile tearing to $\approx 1.5 \sim 2.0$ mm, it does not consider crack growth correction in the J-evaluation method and therefore does not provide η-values derived from LLD measurements. The trends are clear as the present results agree well with the S&T and DNV expressions for $\eta_{J-\mathrm{CMOD}}$ and with the S&T values for $\eta_{J-\mathrm{LLD}}$. Here, we note that our η-factors are slightly lower than the corresponding η-values from other analyses since the present results are derived from plane-strain analyses whereas S&T and DNV F108 employed full 3-D models. Also observe that DNV F108 provides the highest η-values thereby producing nonconservative toughness measurements (larger experimental J-value at a fixed amount of Δa).

Fig. 15 provides a comparison of the elastic compliance between previous Eq. (20) and the elastic analyses described by S&T [9]. The close agreement between both results is evident even though Eq. (20) is based upon plane-strain analyses whereas S&T results derive from 3-D analyses.

A.2. 3P SE(B) specimens

Much recent research has been conducted on developing improved J estimation equations based on CMOD measurements for three-point bend SE(B) specimens, particularly for shallow crack configurations. These investigation efforts include the early work of Kirk and Dodds (K&D) [24], Kim and Schwalbe (K&S) [25], Donato and Ruggieri (D&R) [26] (which is the basis for previous Eqs. (10) and (11)), Davies et al. [38] and Zhu et al. [27] (which is incorporated into last revision of ASTM E1820 standard [15] and ISO 15653 [16]). All these analyses adopt plane strain models of conventional SE(B) specimens with $W/B = 2$.

Fig. 16(a–b) compares factors $\eta_{J-\mathrm{CMOD}}$ and $\eta_{J-\mathrm{LLD}}$ defined by previous Eqs. (10) and (11) with the corresponding results derived from all these investigations. These plot also include the $\eta_{J-\mathrm{CMOD}}$ and $\eta_{J-\mathrm{LLD}}$ expressions from the 3-D analyses of the SE(B) specimens with $W/B = 1$ and $B = 14.8$ mm described in Appendix B (recall that this geometry matches the tested cracked SE(B) configuration). Consider first the $\eta_{J-\mathrm{CMOD}}$ results for the crack configurations with $W/B = 2$ displayed in Fig. 16(a). The η-values are essentially unchanged for almost the entire range of crack size characterized by $0.1 \leq a/W \leq 0.5$; here, only the K&D expression deviates from other analyses providing slightly larger (nonconservative) η-values for deep cracks ($a/W > 0.5$). Now direct attention to the $\eta_{J-\mathrm{CMOD}}$-factors for the SE(B) specimens with $W/B = 1$ (which derive from the 3-D analyses described next in Appendix B). These results are significantly lower than the corresponding plane-strain analyses of the $W/B = 2$ configuration for all a/W-ratios with differences ranging from $\approx 11\%$ for shallow cracks to $\approx 25\%$ for deep cracks. Consider next the $\eta_{J-\mathrm{LLD}}$ results shown in Fig. 16(b). The proposed expression from Zhu et al. [27] is essentially identical to previous Eq. (11) for all crack sizes in the range $a/W \geq 0.25$. However, the 3-D results of $\eta_{J-\mathrm{LLD}}$-factors for the SE(B) specimens with $W/B = 1$ are below the corresponding plane-strain results. Here, a rather surprising behavior displayed by these 3-D results is associated with decreased η-values with increased a/W-ratios for $a/W \geq 0.4$.

Fig. 17 provides a comparison of the elastic compliance between previous Eq. (20) and the results derived from the 3-D elastic analyses for the SE(B) specimen with $W/B = 1$ described in Appendix B. The plot also includes the elastic compliance for this crack configuration from Tada et al. [19]. Again, all analyses are virtually identical for almost the

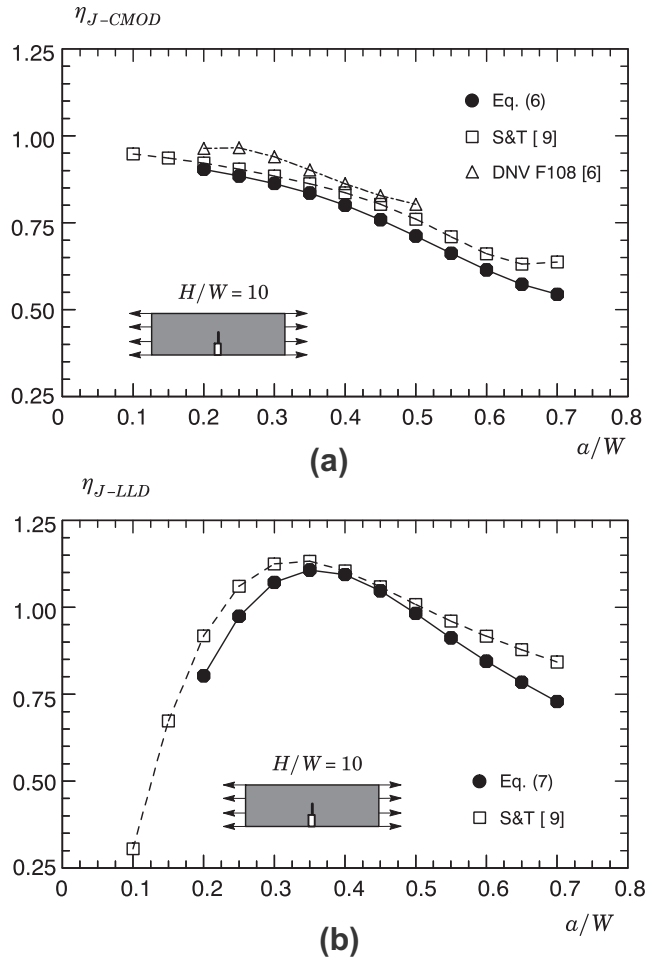

Fig. 14. Comparison of η-factors derived from different analyses, including the present formulations, for clamped SE(T) specimens.

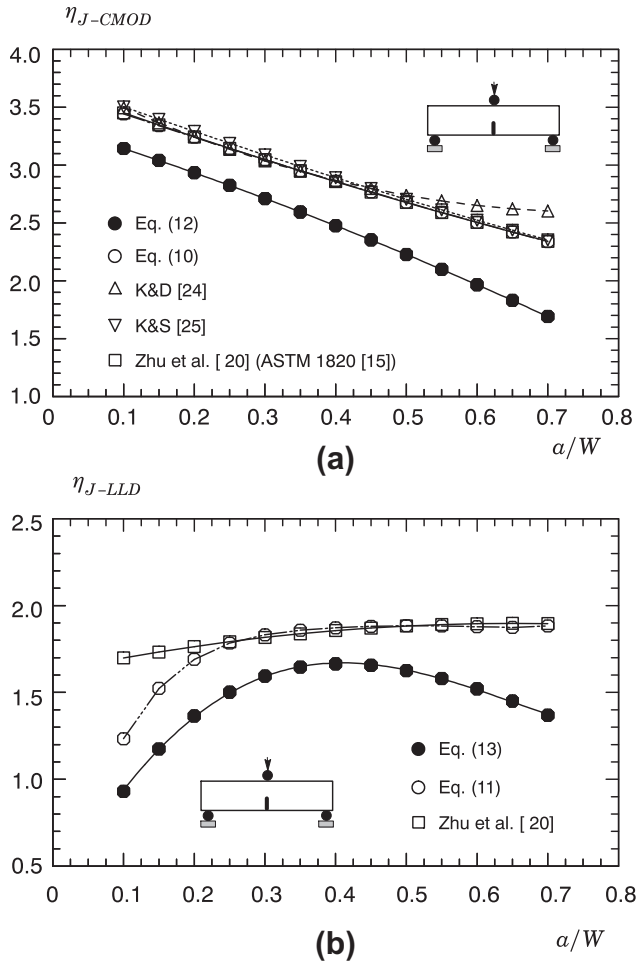

Fig. 16. Comparison of η-factors from different analyses, including the present formulations, for 3P SE(B) specimens.

entire range of crack sizes; here, the 3-D results differ slightly from the plane-strain values only for very shallow cracks ($a/W < 0.2$).

Fig. 14. Comparison of η-factors derived from different analyses, including the present formulations, for clamped SE(T) specimens. Fig. 15. Variation of a/W with normalized elastic compliance, μ, based on different analyses for clamped SE(T) specimens. Fig. 16. Comparison of η-factors from different analyses, including the present formulations, for 3P SE(B) specimens. Fig. 17. Variation of a/W with normalized elastic compliance, μ, based on different analyses for 3P SE(B) specimens.

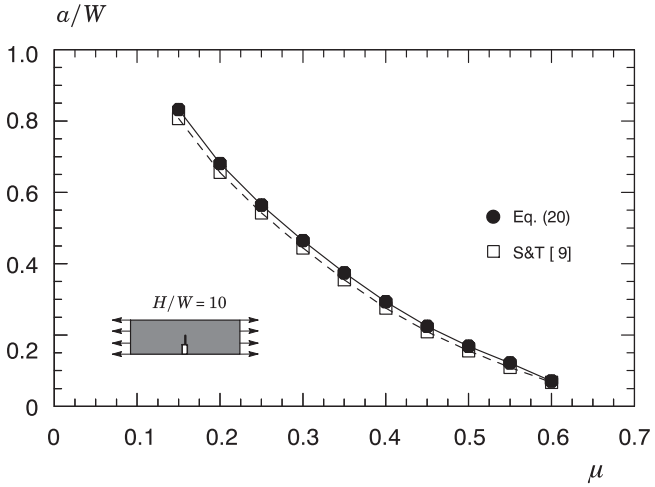

Fig. 15. Variation of a/W with normalized elastic compliance, μ, based on different analyses for clamped SE(T) specimens.

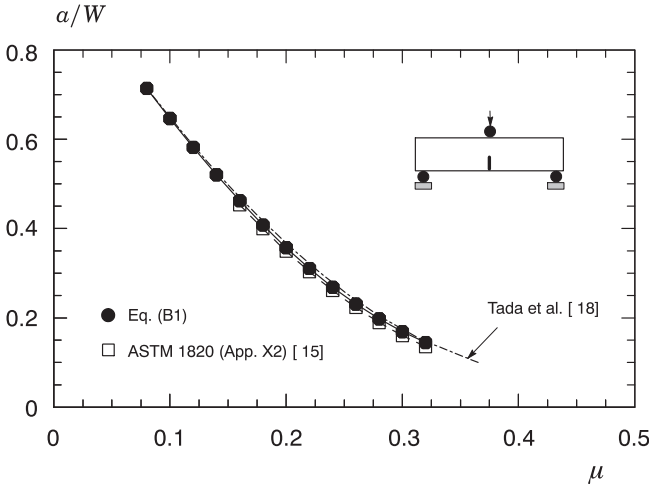

Fig. 17. Variation of a/W with normalized elastic compliance, μ, based on different analyses for 3P SE(B) specimens.

B. η-factors and elastic compliance based on 3-D analysis of SE(B) specimens with square cross section

Although past studies demonstrate a potentially strong interaction of in-plane and thickness effects on crack deformation behavior (thereby affecting the specimen's fracture response), conventional testing programs, including current fracture test standards, to measure experimental J-values and crack extension (Δa) in SE(B) specimens incorporate η-factor and elastic compliance expressions developed for the preferred geometry with $W/B = 2$ under plane-strain conditions. This appendix provides details on the evaluation procedure for J and Δa for SE(B) specimens with square cross section ($W/B = 1$) based on 3-D finite element analyses.

Nonlinear numerical analyses are conducted on finite element models in full 3-D setting for three-point bend SE(B) fracture specimens with thickness, $B = 14.8$ mm, width, $W = 14.8$ mm, and span, $S = 4W$. The analysis matrix covers crack sizes varying from $a/W = 0.1$ to 0.7 with increments of 0.1 (refer to Fig. (2) for the specimen geometry). Fig. 19(a) shows the finite element model constructed for the 3-D analyses of the SE(B) specimen with $a/W = 0.5$. A conventional mesh configuration having a focused ring of elements surrounding the crack front as displayed in Fig. 19(b) is used with a small key-hole at the crack tip where the radius of the key-hole is $\rho_0 = 0.0025$ mm. Symmetry conditions permit modeling of only one-quarter of the specimen with appropriate constraints imposed on the remaining ligament. A typical quarter-symmetric, 3-D model has 25 variable thickness layers with ≈26,000 8-node, 3D elements (≈30,000 nodes) defined over the half-thickness ($B/2$); the thickest layer is defined at $Z = 0$ with thinner layers defined near the free surface ($Z = B/2$) to accommodate strong Z variations in the stress distribution. These finite element models are loaded by displacement increments imposed on the loading points to enhance numerical convergence with increased levels of deformation.

The numerical computations for the cracked configurations at the test temperature reported here are generated using the research code WARP3D [39]. These analyses utilize an elastic–plastic constitutive model with flow theory and conventional Mises plasticity in small geometry change (SGC) setting. The numerical solutions employ a simple power-hardening model to characterize the uniaxial true stress ($\overline{\sigma}$) vs. logarithmic strain ($\overline{\varepsilon}$) in the form $\overline{\varepsilon} = \overline{\sigma}/E$ for $\overline{\sigma} \le \sigma_{ys}$ and $\overline{\varepsilon} = (\sigma_{ys}/E)(\overline{\sigma}/\sigma_{ys})^n$ for $\overline{\sigma} > \sigma_{ys}$, where E is the elastic (longitudinal) modulus, σ_{ys} represents the reference (yield) stress and n is the (Ramberg-Osgood) strain hardening exponent [4,40]. The finite element analyses consider material flow properties covering typical structural, pressure vessel and pipeline grade steels with $E = 206$ GPa and Poisson's ratio, $\nu = 0.3$: $n = 5$ and $E/\sigma_{ys} = 800$ (high hardening material), $n = 10$ and $E/\sigma_{ys} = 500$ (moderate hardening material), $n = 20$ and $E/\sigma_{ys} = 300$ (low hardening material). These ranges of properties also reflect the upward trend in yield stress with the increase in strain hardening exponent, n, characteristic of ferritic structural steels, including pipeline steels. Evaluation of the J-integral derives from a domain integral procedure [39] yielding thickness average values of J which provide a convenient parameter to characterize the average intensity of far field loading on the crack front.

Evaluation of factors $\eta_{J-\mathrm{CMOD}}$ and $\eta_{J-\mathrm{LLD}}$ follows from solving Eq. (1) upon computation of the elastic and plastic components of the J integral, J_e and J_p, with increased loading for a given crack size (as characterized by the a/W-ratio) and strain hardening exponent, n. The research code FRACTUS2D [33] is employed throughout all the computations to determine the η-factors based upon plastic work defined by the plastic component of the area under the load vs. LLD curve or the load vs. CMOD curve. Fig. 18(a–b) provides the η_J-factors derived from CMOD and LLD for the analyzed SE(B) specimens with varying a/W-ratios and different hardening properties. In these plots, the solid symbols correspond to the computed η-values whereas the lines represent polynomial fitting curves to the numerical data. It is seen that the η-values are weakly dependent of strain hardening for the entire range of a/W-ratio. In particular, factors $\eta_{J-\mathrm{CMOD}}$ are essentially insensitive to the strain hardening

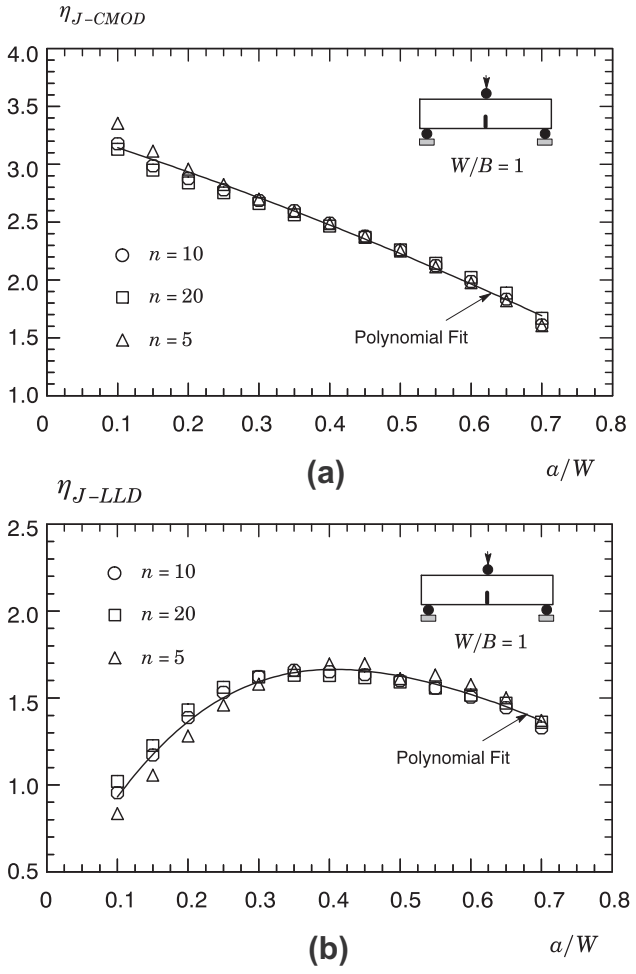

Fig. 18. Variation of plastic factor ηJ with a/W-ratio derived from 3-D finite element analyses of the SE(B) specimens with $W/B = 1$ and varying strain hardening: (a) CMOD-based η-factor; (b) LLD-based η-factor.

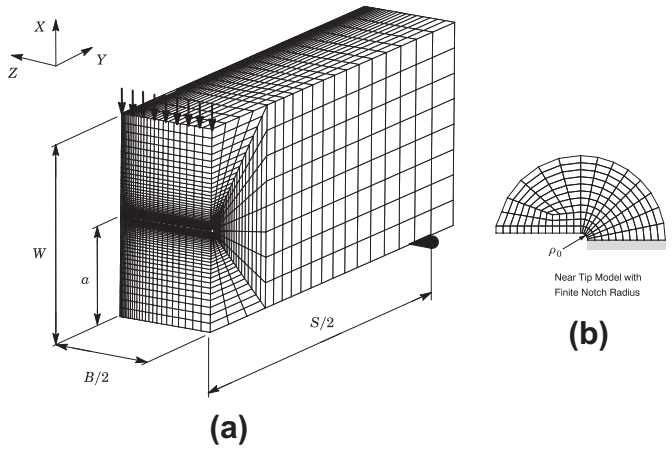

Fig. 19. (a) Finite element model constructed for the 3-D analyses of the SE(B) specimen with $a/W = 0.5$; (b) Small key-hole at the crack tip to model crack blunting.

exponent, n. This last feature bears strong similarity with previous published results (which are presented in previous Appendix A). To provide a simpler manipulation of the previous results aiming at developing testing practices and using the plots displayed in Fig. 18(a–b) for guidance, a functional dependence of factors $\eta_{J-\mathrm{CMOD}}$ and $\eta_{J-\mathrm{LLD}}$ with crack size is constructed yielding Eqs. (12) and (13) already presented in previous Section 2.1.2.

Consider now the variation of applied load with increased crack mouth opening displacement (V or CMOD) for the SE(B) specimen with varying crack size as described by the a/W-ratio. Standard elastic, finite element analyses of the 3-D models for the SE(B) configurations with $W/B = 1$ define the (linear) dependence of applied load, P, on crack mouth opening displacement with different crack length. For a fixed displacement, V, increasing the crack size decreases the specimen stiffness thereby reducing the applied load, P. The slope of the linear evolution of P with V for a given specimen geometry then enables evaluation of the specimen compliance, C_{CMOD}, with crack size to yield the functional dependence of a/W with μ displayed in previous Fig. 17. In that plot, the solid symbols correspond to the numerical results whereas the line represents a 5-th order polynomial fitting using a standard least square procedure which is described by

$$\left[\frac{a}{W}\right]^{\mathrm{SEB}}_{S/W=4} = 1.0172 - 4.2253\mu + 6.9296\mu^2 - 25.9275\mu^3 + 93.5525\mu^4 - 107.7494\mu^5 \tag{B.1}$$

where a/W ranges from 0.1 to 0.7.

Fig. 18. Variation of plastic factor η_J with a/W-ratio derived from 3-D finite element analyses of the SE(B) specimens with $W/B = 1$ and varying strain hardening: (a) CMOD-based η-factor; (b) LLD-based η-factor. Fig. 19. (a) Finite element model constructed for the 3-D analyses of the SE(B) specimen with $a/W = 0.5$; (b) Small key-hole at the crack tip to model crack blunting.

References

[1] Manouchehri S, Howard B, Denniel S. A discussion of the effect of the reeled installation process on pipeline limit states. In: 18th international offshore and polar engineering conference (ISOPE), Vancouver, Canada 2008.

[2] Wästberg S, Pisarski H, Nyhus B. Guidelines for engineering critical assessments for pipeline installation methods introducing cyclic plastic strain. In: 23rd international conference on offshore mechanics and arctic engineering (OMAE), Vancouver, Canada 2004.

[3] Hutchinson JW. Fundamentals of the phenomenological theory of nonlinear fracture mechanics. Journal of Applied Mechanics 1983;50:1042–51.

[4] Anderson TL. Fracture mechanics: fundaments and applications. 3rd ed. Boca Raton, FL: CRC Press; 2005.

[5] Det Norske Veritas. Submarine pipeline systems. Offshore Standard OS-F101 2010.

[6] Det Norske Veritas. Fracture control for pipeline installation methods introducing cyclic plastic strain. DNV-RP-F108 2006.

[7] Cravero S, Ruggieri C. Estimation procedure of J-resistance curves for SE(T) fracture specimens using unloading compliance. Engineering Fracture Mechanics 2007;74:2735–57.

[8] Cravero S, Ruggieri C. Further developments in J evaluation procedure for growing cracks based on LLD and CMOD data. International Journal of Fracture 2007;148:347–400.

[9] Shen G, Tyson WR. Crack size evaluation using unloading compliance in single-specimen single-edge notched tension fracture toughness testing. Journal of Testing and Evaluation 2009;37(4). JTE102368.

[10] Nyhus B, Polanco M, Ørjasæter O. SENT specimens as an alternative to SENB specimens for fracture mechanics testing of pipelines. In: 22nd international conference on ocean, offshore and arctic engineering (OMAE), Vancouver, Canada 2003.

[11] Cravero S, Ruggieri C. Correlation of fracture behavior in high pressure pipelines with axial flaws using constraint designed test specimens – part I: plane-strain analyses. Engineering Fracture Mechanics 2005;72:1344–60.

[12] Silva LAL, Cravero S, Ruggieri C. Correlation of fracture behavior in high pressure pipelines with axial flaws using constraint designed test specimens – part II: 3-D effects on constraint. Engineering Fracture Mechanics 2006;76:2123–38.

[13] Shen G, Bouchard R, Gianetto JA, Tyson WR. Fracture toughness evaluation of high-strength steel pipe. In: ASME PVP 2008 pressure vessel and piping division conference. Chicago, IL: American Society of Mechanical Engineers; 2008.

[14] Park DY, Tyson WR, Gianetto JA, Shen G, Eagleson RS. Evaluation of fracture toughness of X100 pipe steel using SE(B) and clamped SE(T) single specimens. In: 8th international pipeline conference (IPC), Calgary, Canada 2010.

[15] American Society for Testing and Materials. Standard test method for measurement of fracture toughness. ASTM E1820–2011 2011.

[16] International Organization for Standardization. Metallic materials – method of test for the determination of quasistatic fracture toughness of welds. ISO 15653–2010 2010.

[17] Joyce JA. Manual on elastic-plastic fracture: laboratory test procedure. In ASTM manual series MNL 27. ASTM International; 1996.

[18] Ernst HA, Paris PC, Landes JD. Estimations on J-integral and tearing modulus T from a single specimen record. In: Roberts R, editor. Fracture mechanics: thirteenth conference. Philadelphia: ASTM STP 743, American Society for Testing and Materials; 1981. p. 476–502.

[19] Tada H, Paris PC, Irwin GR. The stress analysis of cracks handbook. 3rd ed. American Society of Mechanical Engineers; 2000.

[20] Zhu XK, Leis BN, Joyce JA. Experimentation estimation of J-R curves from load-CMOD record for SE(B) specimens. Journal of ASTM International 2008;5(5). JAI101532.

[21] Joyce JA, Hackett EM, Roe C. Effects of crack depth and mode loading on the J-R curve behavior of a high strength steel. In: Underwood JH, Schwalbe K-H, Dodds RH, editors. Constraint effects in fracture. Philadelphia: ASTM STP 1171, American Society for Testing and Materials; 1993. p. 239–63.

[22] Ruggieri C. Further results in J and CTOD estimation procedures for SE(T) fracture specimens – part I: homogeneous materials. Engineering Fracture Mechanics 2012;79:245–65.

[23] Paredes M, Ruggieri C. Further results in J and CTOD estimation procedures for SE(T) fracture specimens - Part II: weld centerline cracks. Engineering Fracture Mechanics 2012;89:24–39.

[24] Kirk MT, Dodds RH. J and CTOD estimation equations for shallow cracks in single edge notch bend specimens. Journal of Testing and Evaluation 1993;21:228–38.

[25] Kim YJ, Schwalbe K-H. On experimental J estimation equations based on CMOD for SE(B) specimens. Journal of Testing and Evaluation 2001;29:67–71.

[26] Donato GHB, Ruggieri C. Estimation procedure for J and CTOD fracture parameters using three-point bend specimens. In: 6th international pipeline conference (IPC 2006), Calgary, Canada 2006.

[27] Zhu XK, Joyce JA. Revised incremental J-integral equations for ASTM E1820 using the crack mouth opening displacement. Journal of Testing and Evaluation 2009;37(3). JTE102183.

[28] Petti JR, Dodds RH, Link LR. Crack mouth opening displacement-based ηa factors for SE(B) specimens. Journal of Testing and Evaluation 2009;37(4):1–4.

[29] Nevalainen M, Dodds RH. Numerical investigation of 3-D constraint effects on brittle fracture in SE(B) and C(T) specimens. International Journal of Fracture 1995;74:131–61.

[30] Begley JA, Landes JD. The J-integral as a fracture criterion. In: Corten HT, Gallagher JP, editors. Fracture toughness. Philadelphia: ASTM STP 514, American Society for Testing and Materials; 1972. p. 1–20.

[31] American Society for Testing and Materials. Standard test method for linear-elastic plane-strain fracture toughness KIc of metallic materials. ASTM E399–2009 2009.

[32] Savioli RG, Ruggieri C. J and CTOD estimation formulas for C(T) fracture specimens including effects of weld strength overmatch. International Journal of Fracture 2013;179:109–27.

[33] Ruggieri C. FRACTUS2D: numerical computation of fracture mechanics parameters for 2-D cracked solids. Tech. rep. University of Sao Paulo; 2011.

[34] Donato GHB, Magnabosco R, Ruggieri C. Effects of weld strength mismatch on J and CTOD estimation procedure for SE(B) specimens. International Journal of Fracture 2009;159:1–20.

[35] American Petroleum Institute. Fitness-for-service. API RP-579–1/ASME FFS-1 2007.

[36] Steekamp PAJM. J-R curve testing of three-point bend specimen by the unloading compliance method. In: Read DT, Reed RP, editors. Fracture mechanics: eighteenth symposium. Philadelphia: ASTM STP 945, American Society for Testing and Materials; 1988. p. 583–610.

[37] Dzugan J. Crack length calculation by the unloading compliance technique for charpy size specimens. Wissenschaftlich-Technische Berichte FZR-385. Forschungszentrum Rossendorf (FZR); 2003.

[38] Davies CM, Kourmpetis M, O'Dowd NP, Nikbin KM. Experimental evaluation of the J and C^* parameter for a range of cracked geometries. Journal of ASTM 2006;3(4). JAI13221.

[39] Gullerud A, Koppenhoefer K, Roy A, RoyChowdhury S, Walters M, Bichon B, et al. WARP3D: dynamic nonlinear fracture analysis of solids using a parallel computers and workstations, structural research series (SRS 607). UILU-ENG-95-2012, University of Illinois at Urbana-Champaign; 2004.

[40] Dowling NE. Mechanical behavior of materials: engineering methods for deformation, fracture and fatigue. 2nd ed. New Jersey: Prentice Hall; 1999.